# Icosahedron-fcc transition size by molecular dynamics simulation of Lennard-Jones clusters at a finite temperature

Tamio Ikeshoji*,†
*Tohoku National Industrial Research Institute, 4-2-1, Nigatake, Miyagino-ku, Sendai, 983-8551, Japan*

Gérard Torchet and Marie-Françoise de Feraudy
*Laboratoire de Physique des Solides, CNRS/P XI UMR No. 8502, Université Paris-Sud, Bâtiment 510, 91405 Orsay cedex, France*

Kenji Koga*
*National Institute of Materials and Chemical Research, 1-1, Higashi, Tsukuba, Ibaraki, 305-8565, Japan*
(Received 5 July 2000; published 20 February 2001)

We studied finite-temperature ensembles of solid clusters produced by cooling liquid droplets either by evaporation or by a thermostat through a molecular dynamics calculation using the Lennard-Jones potential. The ensembles consist of either single or binary component clusters with 25% of the atoms 8% smaller in diameter than the other 75%. These clusters (380 clusters in total) exhibit various structures in the size range of $n=160-2200$, where $n$ is the number of atoms in a cluster. For increasing size, the clusters show a gradual transition from icosahedral to a variety of structures: decahedral, face centered cubic, a small amount of hexagonal, and some icosahedral structures. They are asymmetrical or faulted. Electron diffraction patterns calculated with average structure factors of clusters after grouping them into several size regions are very similar to those experimentally observed. The size transition is around $n=450$ for single component clusters whatever the cooling process, evaporation or thermostat. This size is smaller than the experimental transition size estimated for argon clusters formed in a supersonic expansion. The transition size for binary component clusters is around $n=600$ for evaporative cooling, and larger for thermostatic cooling. The larger transition size found for the binary component clusters is consistent with the large icosahedral Au-Fe and Au-Cu alloy clusters observed experimentally.

DOI: 10.1103/PhysRevE.63.031101 PACS number(s): 82.20.Wt, 36.40.Ei, 61.46.+w

## I. INTRODUCTION

The structure of an atomic or molecular cluster is a function of not only components and temperature but also the number of atoms in the cluster. Icosahedral (Ih) structures are in many cases the most stable for small sizes. These Ih clusters can be abundantly observed in some cluster sources, giving rise to ''magic numbers.'' Since they have fivefold symmetry, which never appears in bulk except in quasicrystals, they transform into bulk structures, generally with face centered cubic (fcc) close packing, on increase in size. This structural change was observed experimentally by electron diffraction measurements on Ar clusters, formed in vacuum by supersonic expansion, and estimated to occur around $\overline{n}=750$ by Farges *et al.* [1,2], where $\overline{n}$ is the mean number of atoms in a cluster. With similar methods, molecular clusters of $CO_2$ and $N_2$ showed smaller transition sizes [3,4]. A structural change in metal clusters was also observed using electron or x-ray diffraction and high-resolution electron microscopy (HREM), the transition size being dependent on the metallic species [5–7]. Electron microscopy reveals that Mark's decahedral (Dh) clusters are generated in a wide region between icosahedral and fcc rich sizes.

Many theoretical calculations on size-dependent structures and structural change in atomic clusters have been done using the Lennard-Jones (LJ) potential. Reliable calculations of the structure relaxation of ideal Ih and cuboctahedral fcc clusters gave an estimate of the transition size from Ih to fcc as $n=10^4$ [8], where $n$ is the number of atoms in a cluster. This size is, however, very far from the experimentally observed size of disappearance of Ih clusters. Another calculation showed that Ih clusters change at $n=1600$ into Mark's decahedral clusters [9], which produce electron diffraction patterns very similar to those produced by fcc clusters with twin faults. Cleveland and Landman, working on metal clusters, found similar structural sequences and gave related transition sizes [10]. After a detailed analysis of the electron diffraction patterns obtained by Farges *et al.* [1,2] and using a ''plausible'' growth model, van de Waal came to the conclusion that there was no evidence for a size-dependent Ih-fcc structural transition [11] and that fcc clusters including a few crossing-stacking faults were the best candidates for sizes $n \geqslant 500$, with no need to consider Dh clusters [12]. All these calculations were for ideal structures at 0 K. However, in diffraction experiments, the clusters produced are at a finite temperature and distributed in a wide range of sizes and thus cannot be reduced to those with ideal structures that form a sequence of specific atom numbers. A calculation is necessary that includes finite-temperature effect and kinetics for clusters of various sizes. Recent attempts in this direction may be found in Cleveland, Luedtke, and Landman's molecular dynamics (MD) calculation [13] for a fcc Au cluster

*Also at National Institute for Advanced Interdisciplinary Research, 1-1-4, Higashi, Tsukuba, Ibaraki 305-8562, Japan.
†Author to whom correspondence should be addressed. Email address: tamio@tniri.go.jp

 

of $n=459$, which showed the formation of an Ih part on heating the cluster near the melting temperature, and in Baletto, Mottet, and Ferrando's MD calculation for Ag cluster growth [14]. Another example is calculation of the structural change in LJ clusters with a certain number of atoms at finite temperatures among liquid, fcc, and Ih, using Monte Carlo simulation [15], the parallel tempering method [16,17], or MD simulation [18]. Romero, Barrón, and Gómez examined all LJ clusters from $n=147$ to 308, pointing out that some Dh-based clusters are lower in energy than the Ih-based clusters after optimization at 0 K in this size region, although the latter clusters have in most cases the lowest energy [19]. However, these recent calculations were still only performed either at 0 K for clusters of various sizes or at finite temperature for clusters of a few given sizes, and no reliable prediction about the Ih-fcc transition has been presented so far to our knowledge. In this paper, we describe cluster structures formed by cooling liquid droplets of various sizes either by evaporation or by a thermostatic process, using MD simulation of LJ particles. It is well known that, during a supersonic expansion, the rare gas is cooled down, allowing the formation of liquid droplets by condensation of atoms. Droplets are then cooled by evaporation and transform into solid clusters. Our previous MD simulations showed that this evaporation process plays an important role in the appearance of magic numbers in small LJ clusters ($n=13-26$) [20,21]. MD simulation of liquid droplets with constant energy, which leads to the cooling of the droplets by evaporation, should give results comparable with the supersonic experiments. Although it is necessary to have a lot of clusters to achieve good statistics and reliable results, one run includes 70 or 80 samples with different sizes of liquid droplet in the range of $n=220-2700$ ($n=160-2200$ after evaporation) in this paper. A total number of 380 clusters have been examined. In the case of smaller clusters ($n<100$), it is possible to survey a potential energy surface and find many energy minimum structures at 0 K [22]. However, this kind of approach may be difficult for larger clusters because of the exponential increase in the number of local minima. The simulations described in this paper have been carried out under conditions similar to the experimental ones, which may avoid this difficulty. The present work is a first attempt at showing that this kind of calculation is able to predict the structural transitions at finite temperatures as a function of cluster size.

In binary clusters, the Ih-fcc transition may also be a function of the properties of the second component. Icosahedral morphology has been observed with HREM by one of the authors [23–25] for Au–25 at. % Cu and Au–11 at. % Fe clusters up to sizes (several nanometers) larger than those observed for pure Au clusters. Multishell icosahedral clusters become deformed when their size increased because of the increasing difference between atomic distances along radial and tangential directions. This mismatch may be compensated by mixing atoms of different sizes. The Cu and Fe atoms are 11% and 14% smaller than the Au atom, respectively. Binary clusters are produced by cooling a mixture of two metallic vapors with He gas and deposited onto an amorphous carbon sheet. This cooling process, which is generally used to produce metal clusters, may be simulated by a stochastic thermostat in MD calculations. In this paper, Andersen's stochastic thermostat is used [28], in which velocities of randomly selected atoms are changed to completely independent velocities but under the Boltzmann distribution at the desired temperature. Although in metal clusters the interaction potential is expected to be different from the LJ potential, the latter has been used in all cases.

## II. CALCULATIONS

The two-component LJ potential $\phi_{ij}$ between atoms $i$ and $j$ of components $\alpha$ and $\beta$,

$$\phi_{ij}=4\epsilon\left\{\left(\frac{r_{ij}}{\sigma_{\alpha\beta}}\right)^{-12}-\left(\frac{r_{ij}}{\sigma_{\alpha\beta}}\right)^{-6}\right\}, \tag{2.1}$$

was used, where $r_{ij}$ is the distance between atoms $i$ and $j$. All variables denoted by $*$ in this paper are nondimensional with LJ energy $\epsilon$, distance parameter $\sigma_{\alpha\alpha}$ ($>\sigma_{\beta\beta}$), atomic mass, and Boltzmann constant $k_B$. When argon is used as a reference, temperature $T^*=1$, time $t^*=1$, and distance $r^*=1$ correspond to 119.8 K, 2.16 ps, and 0.341 nm, respectively [26]. For the binary component system, atoms having the same mass, the same energy parameter, and a smaller size parameter $\sigma_{\beta\beta}/\sigma_{\alpha\alpha}=0.92$ were randomly added to the system in a 25% proportion. The distance parameter between the different kinds of atom is the average, $\sigma_{\alpha\beta}=(\sigma_{\alpha\alpha}+\sigma_{\beta\beta})/2$

160 single component and 80 binary component liquid droplets with different sizes were prepared under periodic boundary conditions by cooling (to $T^*=0.6$) the center region of a unit cell filled with $n$ ($=220-2700$) LJ particles at $T^*=1.0$, with number density 0.072 in the gas state [27]. The initial number of particles was fixed according to the progression $n^{1/3}=5.95+0.05k$ ($k=1,2,...,160$) or $n^{1/3}=5.9+0.1k$ ($k=1,2,...,80$), respectively. A time step of $\delta t^*=0.01$ was used in all MD calculations. After an equilibration time of $t^*=1000$, each liquid droplet formed was put into a free space and MD calculation was done without any constraint, i.e., under constant energy, up to $t^*=20000$, in order to cool down the clusters by evaporation. Further cooling was necessary to calculate the physical properties at $T^*=0.3$, which corresponds to the estimated temperature 35 K of Ar clusters in supersonic expansion experiments. Thermostatic cooling (for a time of $t^*=1000$) was used to cool down to $T^*=0.3$ after the evaporative cooling. The thermostatic cooling process did not affect the cluster structure. Structure factors calculated at this temperature were then converted into electron diffraction patterns given by $Is^3$ vs $s$, where $I$ is the diffraction intensity and $s$ is the diffraction parameter [$s=(4\pi/\lambda)\sin(\theta/2)$ with electron wavelength $\lambda$ and diffraction angle $\theta$], using the atomic factors and radius of Ar. In the thermostatic cooling process of the liquid droplets without evaporation, a droplet was placed under the same periodic boundary conditions as when the droplet was prepared. The linear decrease of the droplet temperature was

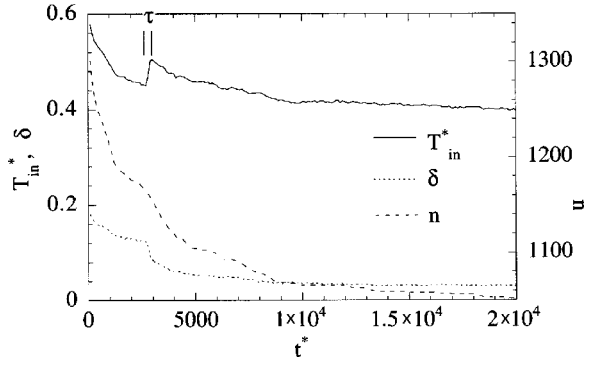


FIG. 1. Changes in inner temperature ($T^*_{\mathrm{in}}$), order parameter ($\delta$), and size ($n$) of a single component liquid droplet as a function of evaporation time ($t^*$); the droplet prepared from 1330 atoms leads to a solid cluster. See text about transition time $\tau$.

controlled from $T^*=0.6$ to 0.3 for time $t^*=30\,000$ by applying a thermostat. The thermostat used was Andersen's stochastic thermostat [28] in all cases. A cluster in the present MD calculations was defined as a group of atoms connected by distances shorter than $r^*=1.5$.

## III. RESULTS AND DISCUSSION

### A. Solidification during cooling

When a liquid droplet is put into free space, evaporation makes its size ($n$) and inner temperature, defined as

$$T_{\mathrm{in}}=\frac{1}{3(n-1)k_B}\sum_{i}^{n}|\mathbf{v}_i-\overline{\mathbf{v}}|^2, \tag{3.1}$$

where $\mathbf{v}_i$ is the velocity of atom $i$ and $\overline{\mathbf{v}}$ is the average velocity of $n$ atoms, decrease together at first, as shown in Fig. 1. At some time in the range of $t^*=1000-20\,000$, the temperature increases suddenly due to the release of the heat of solidification. Solidification at this point is confirmed by the decrease of the order parameter $\delta$, which is defined as the relative root-mean-square interatomic separation [29]

$$\delta=\frac{2}{n(n-1)}\sum_{i<j}\frac{(\langle r_{ij}^2\rangle-\langle r_{ij}\rangle^2)^{1/2}}{\langle r_{ij}\rangle}, \tag{3.2}$$

as also shown in Fig. 1. Clusters get smaller, having 75% of the initial size, and cool down to $T^*=0.34-0.42$ after evaporation time until $t^*=20\,000$, but the evaporation does not stop completely. The time needed by the clusters to solidify ($\tau$ in Fig. 1) seems to depend on the cluster structure that is reached after evaporation. A detailed analysis of the structurization process will be described elsewhere.

### B. Structures and structure factors

Four different evolutions of the structure factors from liquid to solid patterns during the evaporation are shown in Figs. 2(a), 2(b), 2(c), and 2(d), in which the liquid-to-solid change took place around $t^*=2700$, 2000, 2000, and 2300, respectively. The structure factors calculated from the solid clusters formed are similar to those provided by Ih, Dh, fcc, and hcp structures, respectively. In each case, a cluster model with approximately the same size as that reached in the MD calculation but having a perfect structure, namely, icosahedral, Mark's decahedral, cuboctahedral fcc, or spherical hcp, was considered. The corresponding structure factors, calculated at $T^*=0.3$, are given at the top of each set of patterns in Figs. 2(a)–2(d). From comparison between the structure factors provided by ideal clusters and those created from liquids, it is obvious that the latter do not exhibit the ideal structures that are generally assigned as minimum energy structures at 0 K. The thermostatic cooling also leads to imperfect solid structures. While the time evolution of the structure factors shows some peak splitting related to the decrease in temperature, no obvious structural change takes place during the cooling process.

In Figs. 3(a)–3(d) are shown the projections of atomic positions in several solid clusters (at $T^*=0.3$) onto a plane, their structure factors being given in Figs. 2(a)–2(d). Among many other formed clusters, these clusters have been selected because they exhibit fairly perfect structures. Tenfold and fivefold symmetry axes are visible in the projections shown in Fig. 3(a) (Ih) and Fig. 3(b) (Dh), respectively. These symmetry axes are used to assign a structure type to the clusters. The presence of twins and stacking faults is easily detected in most of the fcc clusters [e.g., Fig. 3(c)], producing weak peak splitting (or a shoulder) in the first peak of the structure factors [Fig. 2(c)]. The visible difference between the structure factors of perfect Dh and fcc structures concerns the first peak splitting (remarkable in perfect fcc and weak in Dh) as can be seen in the patterns shown at the tops of Figs. 2(b) and 2(c). Such a splitting in fcc was, however, not clearly found in the clusters formed here, probably due to twins or stacking faults in the fcc clusters [30]. Weak splitting in Dh originates in the presence of twins, since the Dh structure can be considered as a combination of five units of almost fcc crystals through five twins. Dh and fcc structures could be clearly distinguished in the projections and not in the intensity curves. The fivefold symmetry axis in the projection can be used to distinguish them. When this Dh symmetry axis is located very close to or at the edge of the cluster, it is assigned to a fcc cluster including twin faults. The predominant hcp structure is easily confirmed by two peaks [indicated by arrows in Fig. 2(d)] that do not appear in either fcc or Dh structure factors.

Structure factors calculated from the clusters formed show various patterns. Even from liquid droplets with almost the same size, different structure types are found in the solid clusters. In order to see the average features of the structure factors, all the resulting clusters were grouped into eight (or seven) size regions having the same number of clusters. Average structure factors obtained from each subgroup reveal a gradual evolution from Ih to fcc structures, as shown in Figs. 4(a) and 4(b). Each subgroup contains 20 [Fig. 4(a)] or 10 clusters [Fig. 4(b)]. In both cases, the standard deviations $\sigma(n)$ of the mean size $\overline{n}$ lie from 30 to 130 [$\sigma(n)\approx 0.9n^{2/3}$]. These patterns of the structure factors are very similar to those recorded for argon clusters in Refs. [1], [2], [9], and [30]. Experimental electron diffraction patterns recorded from clusters produced with Ar gas pressure $P_0$ are

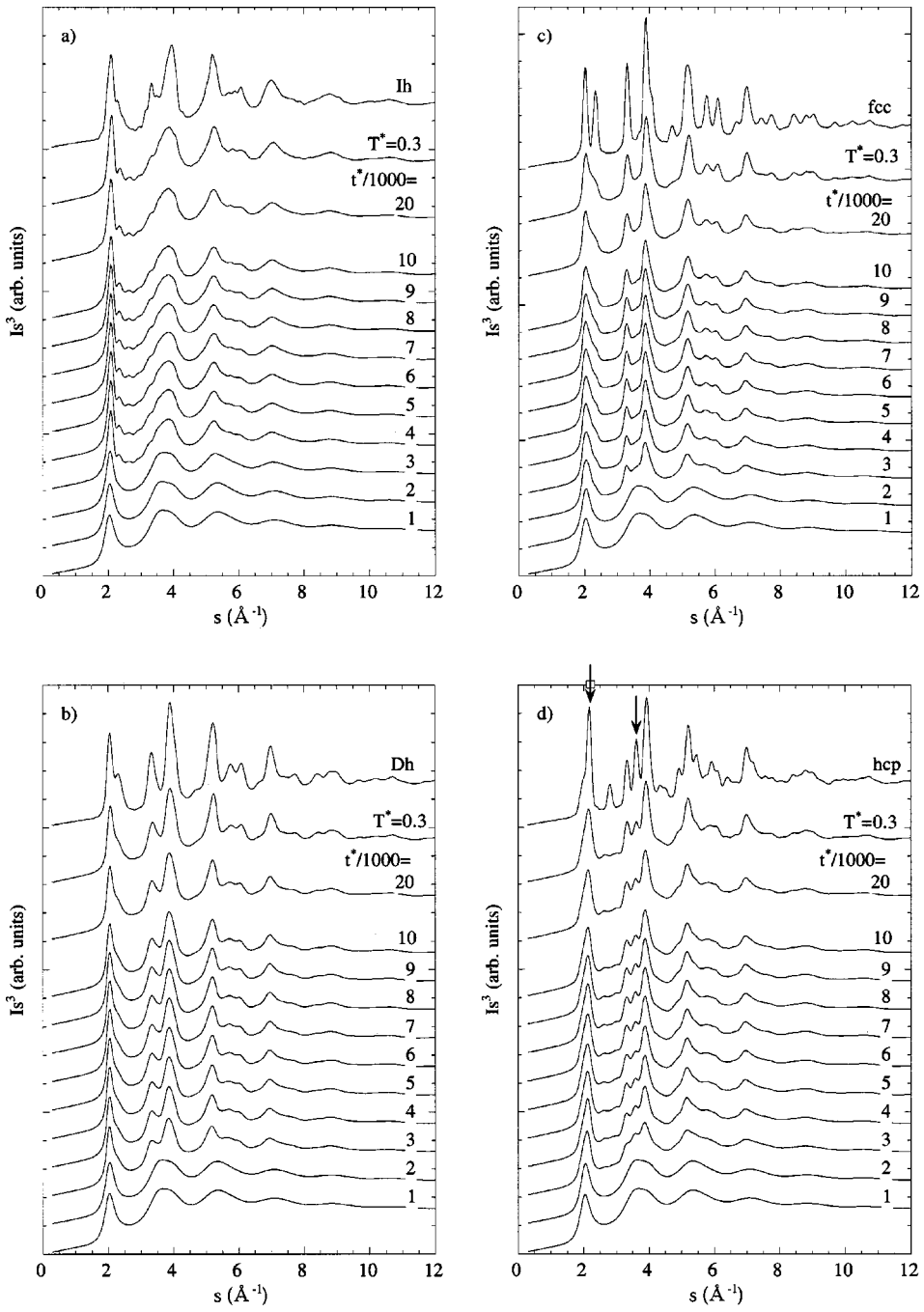


FIG. 2. Structure factors (represented as $Is^3$ vs $s$ of diffraction patterns of Ar) of single component clusters, at successive times $t^*$, during the evaporation of liquid droplets prepared from $n$ atoms. $n=$(a) 1330, (b) 1442, (c) 1124, and (d) 1030. Patterns at $T^*=0.3$ are after further cooling. Top patterns correspond to perfect cluster structures elevated to $T^*=0.3$: (a) icosahedral ($n=1415$), (b) Mark's decahedral ($n=1228$), (c) cuboctahedral fcc ($n=1415$), and (d) spherical hcp ($n=1357$).

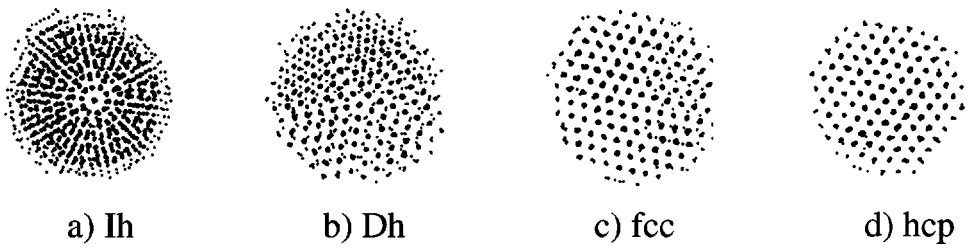


FIG. 3. Atomic structures of single component clusters, (a), (b), (c), and (d) giving the structure factors shown at $T^*=0.3$ in Figs. 2(a), 2(b), 2(c) and 2(d), respectively. (Small dots refer to unstable atoms, i.e., those on the surface.)

superimposed onto several simulated patterns in Fig. 4(a). The superpositions correspond to the best fit between calculated and experimental patterns realized between $s=2.5$ and 10.0 $\text{Å}^{-1}$. The mean cluster size given for the experimental patterns in Fig. 4(a) was estimated through the $n$ vs $P_0$ relationship obtained by using models with icosahedral structure [1,30]. The size distribution of experimentally obtained clusters made of a few hundreds of atoms was estimated to be about $\sigma(n)/n=0.3$ [1]. The superposition displays good agreement between experimental and simulated patterns. Two main differences can be noticed: (i) the experimental first peak is higher, probably due to an instrumental artifact at small diffraction angles; (ii) experimental mean sizes are significantly larger compared to the simulated ones; in particular, the fcc splitting in the second oscillation is visible in the simulated $\bar{n}=470$ pattern while it is hardly detectable in the experimental one at $\bar{n}=670$, which means that the simulation provides smaller-sized fcc clusters. However, the overall agreement between the superimposed patterns shows the reliability of the present simulation and suggests that clusters produced by supersonic expansion may also include some amount of Dh and hcp clusters in the large-size region.

### C. Size dependence of structures

As noted above, the clusters formed do not exhibit perfect structures, but they can be classified into Ih, Dh, fcc, and hcp structures thanks to visualization and structure factors. The ratio of Ih, Dh, fcc, and hcp clusters in the products can be plotted as a function of size as shown in Figs. 5(a)–5(d) for single and binary component clusters produced by either evaporative or thermostatic cooling. The results were obtained from 160, 80, 70, and 70 clusters for Figs. 5(a), 5(b), 5(c), and 5(d), respectively, in the range of $n=160-2200$. These clusters with different sizes were grouped as before in Fig. 4; the 20 samples in each subgroup used for Fig. 5(a) give a $0.23\,(=\sqrt{20}/20)$ precision on each ratio value, and the 10 samples used for Figs. 5(b)–5(d) give a 0.32 precision. Smooth lines connecting data points are only guidelines for the eye. The results shown in Fig. 5(a) were obtained from 160 samples, i.e., two runs forming 80 clusters each. Since these two runs gave almost the same product ratios within $\pm 0.1$ except in a few cases, overall trends seem sufficiently ascertained. While the transition with cluster size from Ih to fcc might be concluded from the change in the average structure factors shown in Fig. 4, the detailed analysis provides a transition from Ih to a variety of structures of Dh, fcc, hcp, and Ih. It occurs around $n=450\pm 100$ for the ensemble of single component clusters after evaporation. Clusters smaller than the transition size are always Ih except in a few cases. When perfect cuboctahedral fcc clusters smaller than $n=309$ are heated up to $T^*=0.35$, they become icosahedral through a solid-solid transition [31]. Therefore, Ih clusters are likely to be absolutely stable at this temperature, although Dh can be the lowest energy structure at some sizes smaller than $n=309$ [19] at 0 K. As the Ih structure seems to be in a wide funnel in the potential energy surface of small-sized clusters, other structures like the tetragonal one, which

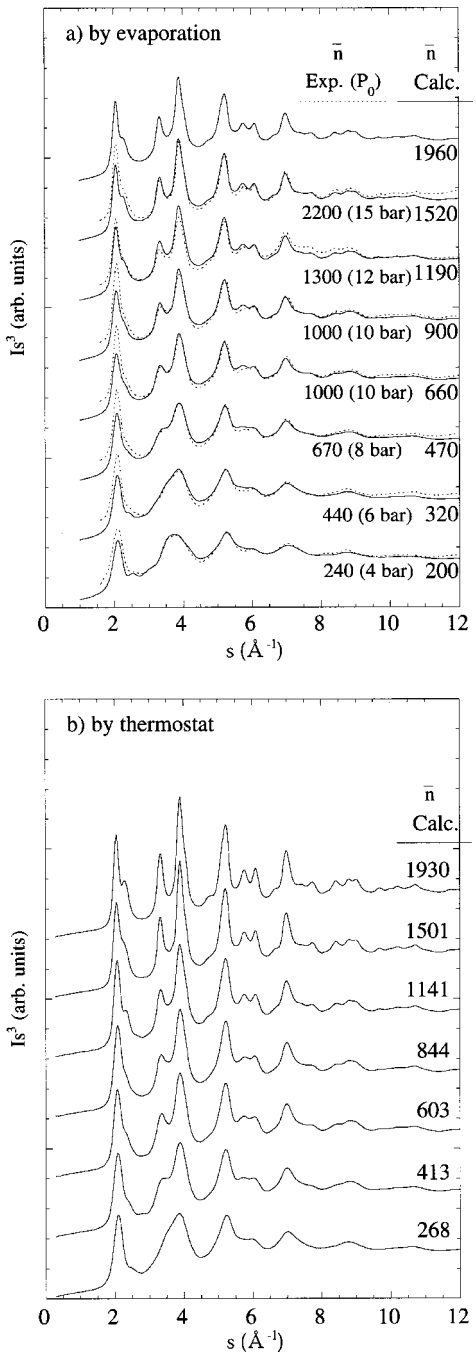


FIG. 4. Average structure factors (represented as $Is^3$ vs $s$ of diffraction patterns of Ar) from single component clusters at $T^*=0.3$. Each calculated pattern is the average of a subgroup including 20 (a) or 10 (b) different sized clusters of mean size $\bar{n}$ with standard deviation $\sigma(n)$ $(\approx 0.9n^{2/3})$. Superimposed dotted lines represent experimentally observed patterns after supersonic expansion of Ar with pressure $P_0$ [30].

was found to be the global minimum structure at $n=96$ [32], are not observed in the present finite-temperature calculation.

The transition size observed here could correspond to the size $n=500$, which was assigned as the starting size of the gradual transition to fcc by a ''plausible'' growth model [12]. According to this model, hcp and Dh are not expected to be produced, while a small amount of hcp and some Dh

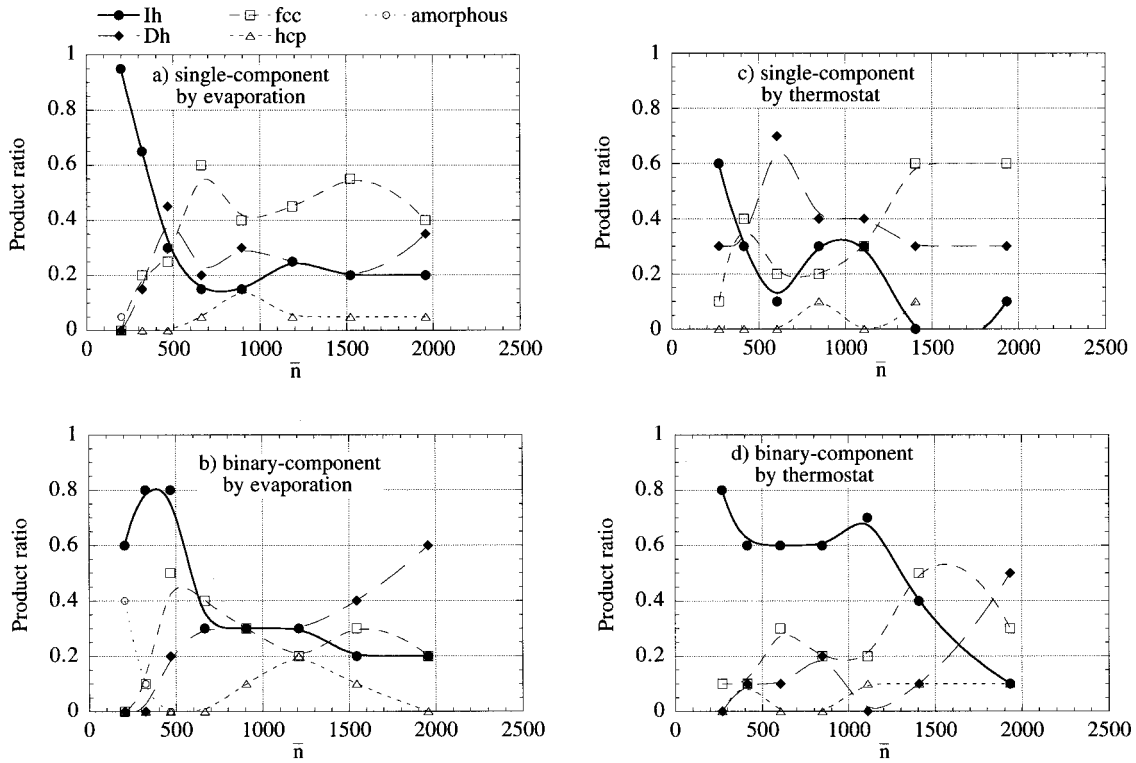


FIG. 5. Product ratio of various structures found in single and binary component clusters by evaporation and thermostatic cooling. Each point is a ratio calculated over 20 products in (a) and 10 in (b)–(d) at mean size $\bar{n}$. Ensembles of clusters in (a) and (c) are identical to those in Figs. 4(a) and 4(b), respectively. See standard deviations given in Fig. 4.

clusters were produced in the present calculation. The transition size obtained here, $n=450$, is smaller than the experimental estimate, $\bar{n}=750$ [1], as shown in Fig. 4(a). One reason for this discrepancy may be the difference between the LJ potential and the real interaction potential of argon atoms. There is obviously a dependence between the potential and the transition size [10,33]. Another and more physical reason for the discrepancy is the slightly different mechanisms leading to solid cluster formation. Cluster growth by a condensation-evaporation process, which may be involved in the real supersonic beam, is not considered in the evaporation sequence of the present simulation. Nevertheless the thermostatic cooling under periodic boundary conditions allows a condensation process, in principle, but the number of free atoms remains limited in the simulation cell used. The same transition size was observed through thermostatic and the evaporative cooling. It implies a weak dependence on the cooling method, at least for cooling rates similar to those used in the present simulation. This calculation did provide a transition size that is not too far from the experimental observation and markedly closer than the size values derived from previous calculations.

The structural transition for the binary component clusters is also from Ih to a variety of structures of Dh, fcc, hcp, and Ih. The transition size is at $n=600\pm100$ for clusters obtained by evaporation and at a much larger size, $n=500-1500$, for clusters obtained by thermostatic cooling. The larger transition size for binary component clusters than for single component ones is consistent with the large icosahedral Au-Fe and Au-Cu alloy clusters observed experimentally [23–25]. The present simulation shows the importance of the difference between the atomic radii of the components.

### D. Potential energy of clusters

When the potential energy per atom, $E_p/n$, is plotted against $n^{-1/3}$, all the data points referring to clusters with different structures formed by evaporation lie almost on the same straight line, expressed as

$$E_p/n=a+bn^{-1/3} \quad (E_p=an+bn^{2/3}), \tag{3.3}$$

where $a$ and $b$ are constants, as shown in Fig. 6(a). In the case of thermostatic cooling, the potential energy of Ih clusters lies on a different line from that of the other (Dh and fcc) clusters as shown in Fig. 6(b). The potential energy of Dh, fcc, and hcp clusters lies on almost the same line. Presumably, the evaporation process removes those surface atoms that are located at unstable positions. The potential energies per atom of Ih and Dh-fcc-hcp clusters after thermostatic cooling cross at $n=420\pm200$, which is very close to the transition size between Ih and Dh-fcc-hcp clusters shown in Fig. 5. However, the crossing size cannot be determined with any precision due to the small difference between the slopes of the lines.

### E. Surface segregation

In the icosahedron, atomic distances in both the radial and tangential directions are larger at the edge than at the center.

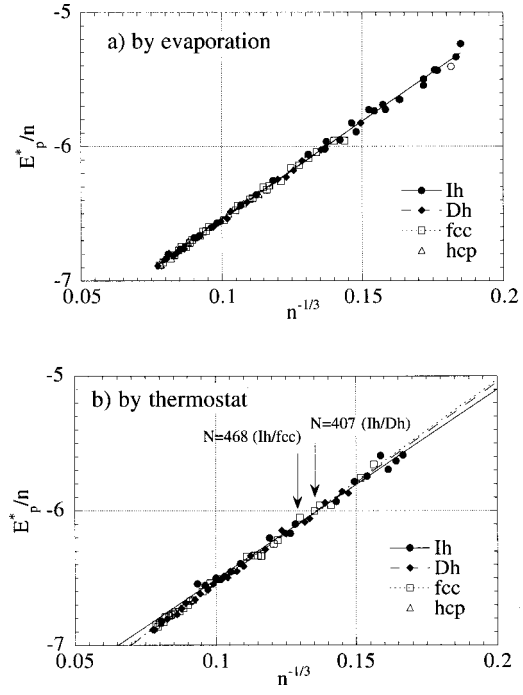


FIG. 6. Potential energy $E_p$ per atom of single component clusters at $T^*=0.3$ as a function of $n^{-1/3}$. Crossing values between different structures are indicated.

Therefore, in binary clusters, if the larger-sized atoms are rather located at the edges and the smaller-sized ones at the center, it should reduce the surface energy and achieve a higher stability. Such localizations are found in binary component clusters in both solid and liquid states, as shown in Figs. 7(a)–7(c). This is similar to what is known as surface segregation [34].

Since a lower concentration of smaller-sized atoms is achieved at the surface region even in clusters cooled under periodic boundary conditions [Fig. 7(c)], surface segregation is not due to the evaporation of selected atoms. Recent calculations for Ar-Xe and Ar-Kr clusters of $n=200-1000$ also showed a surface segregation and different cluster structures because of the difference in size and energy parameters of the LJ potential [36]. In the present simulation, a small difference in the size parameters produced very similar structures in both single and binary component clusters, but led to different transition sizes between structures. Such results imply that the large icosahedral structures observed in clusters made of Au-Cu and Au-Fe alloys [23–25], which give a solid solution in bulk material [35], are due to the difference in size between the two components. Appropriate combination of atoms with different sizes and concentrations would give larger Ih clusters than those observed so far.

## IV. CONCLUSION

The Ih to fcc structural transition observed in experiments on increasing the cluster size was confirmed as a gradual transition from Ih to a variety of ''imperfect'' Dh, fcc, hcp, and Ih structures. Average structure factors calculated from simulated clusters in the range $n=160-2200$ are very similar to those observed in electron diffraction patterns of Ar clusters formed by supersonic expansion. Although MD calculations using a single component LJ potential provide a transition size smaller than that observed experimentally, they prove to give a better estimate than the structure optimization performed previously at 0 K on cluster models with ideal structures. It was also shown that the combination of different sized atoms accounts well for the large icosahedral clusters observed experimentally in binary component (alloy) clusters.

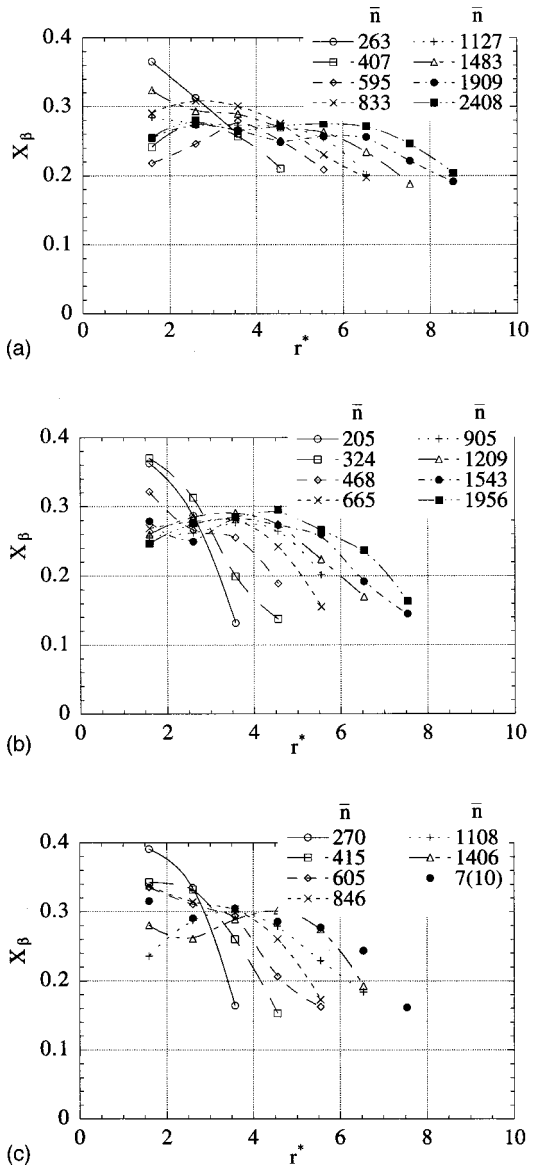


FIG. 7. Average concentration ($X_\beta$) profiles of the smaller-sized LJ particles with $\sigma_{\beta\beta}=0.92$, in binary component clusters of mean size $\bar{n}$, as a function of position $r^*$ from the center of mass. (a) Liquid droplets, (b) solid clusters formed by evaporation, and (c) solid clusters formed by thermostatic cooling.

## ACKNOWLEDGMENT

A DEC AlphaServer 8400 with eight CPUs in the National Institute for Advanced Interdisciplinary Research was used for calculations.

[1] J. Farges, M.-F. de Feraudy, B. Raoult, and G. Torchet, J. Chem. Phys. **84**, 3491 (1986).
[2] J. Farges, M.-F. de Feraudy, B. Raoult, and G. Torchet, Adv. Chem. Phys. **70**, 45 (1988).
[3] G. Torchet, M.-F. de Feraudy, A. Boutin, and A. H. Fuchs, J. Chem. Phys. **105**, 3671 (1996).
[4] F. Calvo, G. Torchet, and M.-F. de Feraudy, J. Chem. Phys. **111**, 4650 (1999).
[5] C. L. Cleveland, U. Landman, T. G. Schaaff, M. N. Shafigullin, P. W. Stephens, and R. L. Whetten, Phys. Rev. Lett. **79**, 1873 (1997).
[6] D. Reinhard, B. D. Hall, P. Berthoud, S. Valkealahti, and R. Monot, Phys. Rev. Lett. **79**, 1459 (1997).
[7] K. Koga, H. Takeo, T. Ikeda, and K. Ohshima, Phys. Rev. B **57**, 4053 (1998).
[8] W. van de Waal, J. Chem. Phys. **90**, 3407 (1989).
[9] B. Raoult, J. Farges, M.-F. de Feraudy, and G. Torchet, Philos. Mag. B **60**, 5067 (1989).
[10] C. L. Cleveland and U. Landman, J. Phys. Chem. **94**, 7376 (1991).
[11] B. W. van de Waal, Phys. Rev. Lett. **76**, 1083 (1996).
[12] B. W. van de Waal, J. Chem. Phys. **98**, 4909 (1993).
[13] C. L. Cleveland, W. D. Luedtke, and U. Landman, Phys. Rev. Lett. **81**, 2036 (1998).
[14] F. Baletto, C. Mottet, and R. Ferrando, Phys. Rev. Lett. **84**, 5544 (2000).
[15] J. P. K. Doye, D. J. Wales, and M. A. Miller, J. Phys. Chem. **109**, 8143 (1998).
[16] J. P. Neirotti, F. Calvo, D. L. Freeman, and J. D. Doll, J. Phys. Chem. **112**, 10 340 (2000).
[17] F. Calvo, J. P. Neirotti, D. L. Freeman, and J. D. Doll, J. Phys. Chem. **112**, 10 350 (2000).
[18] B. G. Moore and A. A. Al-Quraishi, Chem. Phys. **252**, 337 (2000).
[19] D. Romero, C. Barrón, and S. Gómez, Comput. Phys. Commun. **123**, 87 (1999).
[20] T. Ikeshoji, B. Hafskjold, Y. Hashi, and Y. Kawazoe, Phys. Rev. Lett. **76**, 1792 (1996).
[21] T. Ikeshoji, B. Hafskjold, Y. Hashi, and Y. Kawazoe, J. Chem. Phys. **105**, 5126 (1996).
[22] J. P. K. Doye, M. A. Miller, and D. J. Wales, J. Chem. Phys. **111**, 8417 (1999).
[23] K. Koga, D. K. Saha, and H. Takeo, in *Similarities and Differences between Atomic Nuclei and Clusters*, edited by Y. Abe, I. Arai, S. M. Lee, and K. Yabana, AIP Conf. Proceedings No. 416 (AIP, Woodbury, NY, 1997), p. 431.
[24] D. K. Saha, K. Koga, and H. Takeo, Nanostruct. Mater. **8**, 1139 (1997).
[25] D. K. Saha, K. Koga, and H. Takeo, Eur. J. Phys. **9**, 539 (1999).
[26] G. C. Maitland and E. B. Smith, Mol. Phys. **22**, 861 (1971).
[27] T. Ikeshoji and B. Hafskjold, Mol. Phys. **81**, 251 (1994).
[28] H. C. Andersen, J. Chem. Phys. **72**, 2384 (1980).
[29] D. J. Wales and R. S. Berry, J. Chem. Phys. **92**, 4283 (1990).
[30] M.-F. de Feraudy and G. Torchet, J. Cryst. Growth **217**, 449 (2000).
[31] T. Ikeshoji (unpublished).
[32] R. H. Leary and J. P. K. Doye, Phys. Rev. E **60**, R6320 (1999).
[33] J. Xie, J. A. Northby, D. L. Freeman, and J. D. Doll, J. Chem. Phys. **91**, 612 (1989).
[34] See, e.g., Yu Wenbin and D. Stroud, Phys. Rev. B **56**, 12 243 (1997).
[35] T. B. Massalski, *Binary Alloy Phase Diagrams* (ASM International, Metals Park, OH, 1990), pp. 358, 367.
[36] H. Vach, Phys. Rev. B **59**, 13 413 (1999).